physica status solidi b
www.pss-b.com

Magnetoelectric Properties of $Co_{1-x}Ni_xFe_2O_4/BaTiO_3$ Heterostructures with 3–3 Connectivity Obtained by Eutectic Crystallization

*Martin Breitenbach, Kathrin Dörr, and Stefan G. Ebbinghaus**

Multiferroic composites consisting of 62 mol% ferroelectric $Ba_{0.97}Sr_{0.03}TiO_3$ and 38 mol% ferrimagnetic $Co_{1-x}Ni_xFe_2O_4$ with Ni substitution levels of $x = 0$, 0.25, 0.50, 0.75, and 1.00 are obtained from eutectic crystallization in a floating zone furnace. Scanning electron microscopy reveals the self-organized formation of a 3–3 network. Epitaxy of the two phases is confirmed by single-crystal X-ray diffraction. All samples, except the one containing pure $NiFe_2O_4$, are free of impurity phases. The influence of the substitution level x on the unit cell parameters of both materials is investigated by Rietveld refinement before and after a reoxidation process in flowing oxygen at 1173 K. The amount of oxide defects is determined by thermal analysis, showing a nearly constant value throughout the whole $Co_{1-x}Ni_xFe_2O_4$ series. The effect of Ni substitution on the magnetic properties (saturation magnetization and magnetic transition temperature) of the eutectics is investigated. The magnetoelectric (ME) properties of the samples are studied in dependence on the DC field (H_{DC}), the frequency of the AC field (H_{AC}), and temperature. The Ni content has a strong influence on the absolute value of the ME coefficient (α_{ME}), but only a slight effect on the general behavior of the ME properties.

1. Introduction

The magnetoelectric (ME) effect, that is, control of the electrical polarization by a magnetic field (direct ME effect)[1–4] or control of the magnetization by an electric field (converse ME effect),[3,5] was first experimentally verified by Astrov in 1960.[1] Since that time ME materials have attracted huge interest because of their great potential for a variety of applications including data storage and sensors.[2,6] Composite materials consisting of a ferro- or ferrimagnetic and a ferroelectric component[7–11] are of special importance because they often show a much higher ME response than single-phase multiferroics and the ME effect can occur at room temperature.[12] The two components may be connected in various dimensionalities, e.g., as particles in a matrix (0–3 connectivity) or as alternating layers (2–2 connectivity). Whereas these connectivities have been studied extensively, only few articles deal with 3–3-structures, i.e., the ferroelectric and magnetic phase forming 3D meandering structures. This connectivity results from self-organization during the eutectic crystallization of, e.g., $CoFe_2O_4$/$BaTiO_3$ (CFO/BTO) melts as first observed by Van den Boomgaard et al. in the early 1970s.[13,14] Although this approach was one of the first to yield multiferroic composites, it was surprisingly not further studied until, almost 30 years later, Echigoya made use of it again.[15] In the early work of Van den Boomgaard, the Bridgman technique was used, whereas Echigoya chose the floating zone crystal growth instead. Unfortunately, they did not report any ME measurements. Recently, a containerless microwave melting/crystallization has been applied to $CoFe_2O_4/BaTiO_3$ mixtures with 50, 60, and 70 wt% $CoFe_2O_4$, leading to composites containing small amounts of impurities.[16] For an eutectic sample obtained by this approach, a magnetodielectric effect was observed, i.e., the permittivity increased linearly by ≈0.3% for magnetic fields between 0 and ±4 T.[17]

In the course of our research on multiferroic heterostructures with different connectivities,[9,18] we became interested in 3–3 composites. In an earlier publication, we reported on the successful growth of phase-pure $CoFe_2O_4/BaTiO_3$ composites via floating zone melting.[19] As it turned out, the two major obstacles were the formation of the hexaferrite $BaFe_{12}O_{19}$ and of hexagonal $BaTiO_3$. Impurities of $BaFe_{12}O_{19}$ can successfully be avoided using flowing nitrogen as atmosphere during the floating zone process, whereas the formation of the nonferroelectric hexagonal modification of $BaTiO_3$ can be suppressed by a slight Sr substitution (3 mol%). The resulting multiferroic composite had the composition $(CoFe_2O_4)_{0.38}/(Ba_{0.97}Sr_{0.03}TiO_3)_{0.62}$. As a

M. Breitenbach, Prof. S. G. Ebbinghaus
Institute of Chemistry
Martin Luther University Halle-Wittenberg
Kurt-Mothes-Straße 2, D-06120 Halle/Saale, Germany
E-mail: stefan.ebbinghaus@chemie.uni-halle.de

Prof. K. Dörr
Institute of Physics
Martin Luther University Halle-Wittenberg
Von-Danckelmann-Platz 3, D-06120 Halle/Saale, Germany

The ORCID identification number(s) for the author(s) of this article can be found under https://doi.org/10.1002/pssb.201900618.

DOI: 10.1002/pssb.201900618

consequence of the oxygen-free atmosphere during crystallization, the as-grown samples were electrically conductive due to a high degree of oxygen defects. A very strong enhancement of the resistance (>20 MΩ) was achieved by a reoxidation step in air at 973 K. A comprehensive characterization of the ME properties with regard to different crystallization rates, sample thicknesses, and sample alignment has been published.[20] Furthermore, the influence of the static magnetic field (H_{DC}), the frequency of the driving field (H_{AC}), and temperature on the ME properties have been studied. High-resolution scanning transmission electron microscopy (HR-STEM) investigations revealed void-free $CoFe_2O_4/BaTiO_3$ interfaces. An epitaxial relationship between the perovskite and the spinel phase was verified by single-crystal X-ray diffraction (XRD).

Because the approach of eutectic crystallization so far has been used only for $CoFe_2O_4$ as ferrimagnetic material, the aim of this work was the stepwise substitution of Co by Ni in $Co_{1-x}Ni_xFe_2O_4/Ba_{0.97}Sr_{0.03}TiO_3$ eutectics. The magnetostriction of nickel ferrite is much smaller than the one of $CoFe_2O_4$.[21] Nevertheless, strong ME coupling with α_{ME} values in the range of 30–70 mV cm^{-1} Oe^{-1} has been reported for epitaxial films, making $NiFe_2O_4/BaTiO_3$ an interesting system to study.[22]

In this work, the influence of nickel substitution on the unit cell parameters and ME properties of $Co_{1-x}Ni_xFe_2O_4/Ba_{0.97}Sr_{0.03}TiO_3$ eutectics was investigated. Thermogravimetry was used to calculate the amount of oxygen defects in the as-grown samples from the mass gain during reoxidation, which also revealed unexpected changes in the magnetic behavior upon oxygen annealing.

2. Results and Discussion

2.1. Crystal Growth, Scanning Electron Microscopy, and XRD

Crystallization of the $Co_{1-x}Ni_xFe_2O_4/Ba_{0.97}Sr_{0.03}TiO_3$ eutectics proceeded without severe problems for all compositions and resulted in cylindrical boules of 6–8 mm diameter, 50–70 mm length, and 9–13 g weight. With higher Ni amounts, a linearly increasing lamp power had to be applied during the floating zone melting (from 38% for $x = 0$ to 40% for $x = 1$). As an example for the interpenetration of the two components, **Figure 1** shows a scanning electron microscopy (SEM) image of the $Co_{0.5}Ni_{0.5}Fe_2O_4/Ba_{0.97}Sr_{0.03}TiO_3$ sample. During the eutectic crystallization, well-defined geometric structures form by self-organization, resulting in a network that corresponds to a 3–3 connectivity. Such "Chinese script"-type microstructures are typical for directionally solidified eutectic oxides.[23] Energy-dispersive X-ray spectroscopy (EDX) analysis shows that the dark and pale gray regions correspond to the spinel and perovskite phase, respectively. The quantitative evaluation at different spots gave no hints for significant incorporations of Fe, Ni, or Co in the $BaTiO_3$ matrix nor Ti in the spinel phase in agreement with the XRD results discussed later.

To investigate the orientational relationship of the two components, a rectangular-shaped piece (≈200 × 200 × 100 µm) of the sample with $x = 0.5$ was subjected to single-crystal XRD. **Figure 2** shows the reciprocal $hk0$ lattice plane. Points corresponding to the perovskite and spinel phase can easily be distinguished by

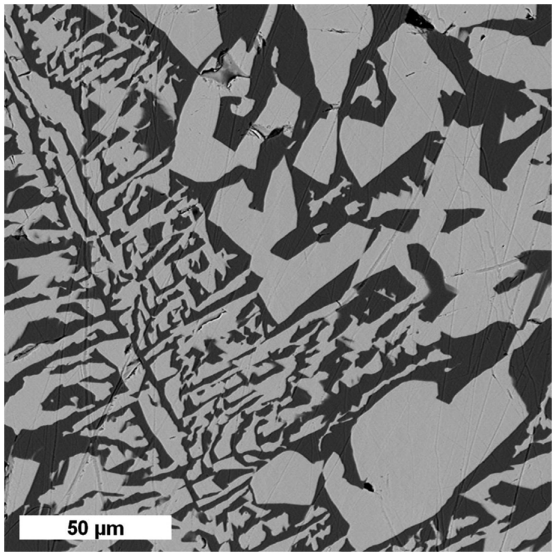

Figure 1. SEM image of a polished slice from the sample with $x = 0.5$.

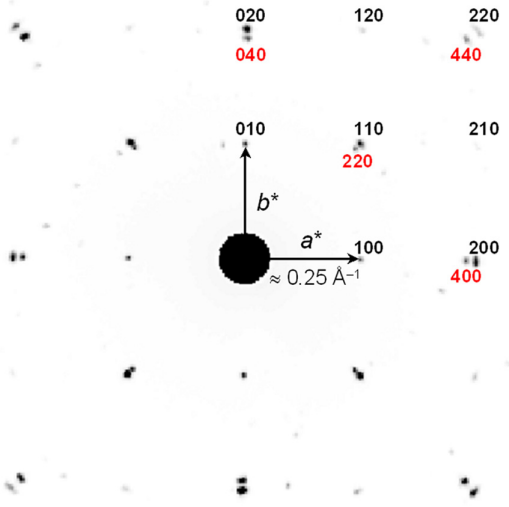

Figure 2. Reconstructed $hk0$-plane of the reciprocal lattice of the $Co_{0.5}Ni_{0.5}Fe_2O_4/Ba_{0.97}Sr_{0.03}TiO_3$ crystal. For h, $k \geq 0$, the points of the perovskite and the spinel are labeled in black and red.

their different d^* values and the systematic reflection conditions for $Co_{0.5}Ni_{0.5}Fe_2O_4$ ($0k0$: $k = 4n$, $h00$: $h = 4n$, $hk0$: $h + k = 4$, $h = 2n$, $k = 2n$). As expected, the sample consists of more than one domain leading to additional peaks (e.g., visible close to the perovskite 010). Nevertheless, the arrangement of reciprocal lattice points clearly evidences the epitaxial orientation spinel(001)[100]||perovskite(001)[100]. This epitaxy was already found by Echigoya on atomic scale via electron diffraction.[15] For floating zone crystallized $CoFe_2O_4/Ba_{0.97}Sr_{0.03}TiO_3$, we confirmed the same epitaxial relationship by HR-STEM in a previous study.[20] Our current XRD investigations now prove that the orientational relationship between the spinel and the perovskite components extends over a much larger length scale in the order of 100 µm.

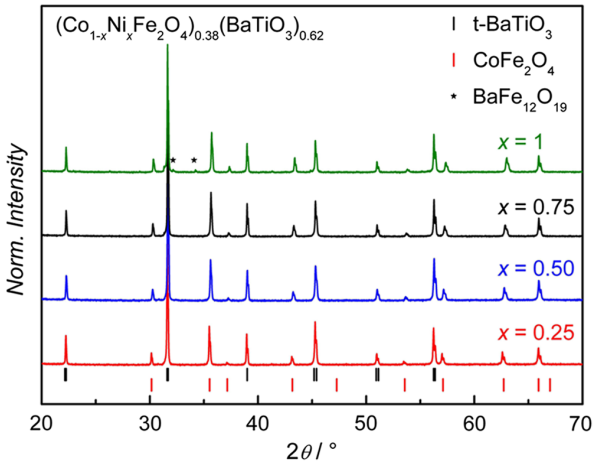

Figure 3. Powder XRD patterns of the different samples after oxygen annealing.

For each sample, two slices (as-grown and reoxidized) were ground into fine powders and subjected to XRD. The resulting powder diffraction patterns of the reoxidized samples are shown in **Figure 3**. The patterns of the as-grown samples were basically identical and are therefore not shown.

All as-grown and oxygen-annealed composites consist solely of $Co_{1-x}Ni_xFe_2O_4$ and $BaTiO_3$. Only in the sample-containing pure $NiFe_2O_4$ ($x = 1$), small traces of $BaFe_{12}O_{19}$ were detected, which were already present before the reoxidation process. Although the conditions during the postannealing had to be harsher than in our earlier experiments, no additional $BaFe_{12}O_{19}$ impurities emerged.

The unit cell parameters of all as-grown and reoxidized samples were obtained from Rietveld refinements. Because the octahedrally coordinated Ni^{2+} ion has a smaller radius than Co^{2+} (0.690 Å vs 0.745 Å[24]), a decrease in the unit cell dimensions is expected. Because $CoFe_2O_4$ and $NiFe_2O_4$ crystallize in the (partially) inverse spinel structure, the tetrahedral sites are predominantly occupied by Fe^{3+} ions and thus their influence can be neglected. The lattice parameters of the $Co_{1-x}Ni_xFe_2O_4$ component are shown in **Figure 4**. A linear decrease in the cell parameters with rising Ni content is observed in accordance with Vegard's law. This behavior was already reported in the literature for powder samples of the $Co_{1-x}Ni_xFe_2O_4$ system.[25] For our composites, the linear behavior indicates that the composition of the ferrite component is very close to the nominal one. Upon reoxidation, a significant decrease in the cell parameter a by an average value of 0.014 Å is observed. This behavior can be explained by the healing of oxygen defects, correlated with the oxidation of Fe^{2+} to Fe^{3+} ions, which are smaller in size ($Fe^{2+}_{(IV)}$: 0.630 Å, $Fe^{3+}_{(IV)}$: 0.490 Å, $Fe^{2+}_{(VI)}$: 0.780 Å, $Fe^{3+}_{(VI)}$: 0.645 Å).[19]

The cell parameters of the $Ba_{0.97}Sr_{0.03}TiO_3$ component are shown in **Figure 5**. A tetragonal unit cell was found, indicating that the ferroelectric $BaTiO_3$ modification (space group *P4mm*) is formed. The ratio c/a is rather small (about 1.001) but nonetheless significant, as shown by the error bars in Figure 5. Attempts to refine the XRD pattern with a cubic unit cell led to far worse χ^2 values. In addition, a strong enhancement of the ME effect after poling the samples in an electric field (see Section 4) also proves the presence of the ferroelectric phase.

With rising Ni content in the spinel component, the cell parameters of $BaTiO_3$ (a_{BTO} and c_{BTO}) of the as-grown samples remain almost constant, whereas, for the corresponding reoxidized samples, a slight decrease in both a_{BTO} and c_{BTO} seems to occur with increasing x. On the other hand, the change is very small (in the order of 0.002 Å corresponding to 0.5‰) which indicates that only traces of Fe, Co, or Ni are incorporated into the perovskite phase during the floating zone melting. This interpretation is corroborated by previous SEM/EDX and TEM/EDX measurements, in which no significant signals for these elements were detected in the $BaTiO_3$ component.[19,20] Furthermore, earlier investigations on sintered ceramics have shown that the solubility of Fe, Co, and Ni in the cubic/tetragonal modification of $BaTiO_3$ is well below 1%.[26]

Upon annealing in oxygen, both a_{BTO} and c_{BTO} decrease by roughly 0.0035 Å again due to healing of oxygen defects leading to an oxidation of Ti^{3+} to the smaller Ti^{4+}. The change in the unit cell parameters is about one quarter of the change of $a_{ferrite}$ reflecting the higher electropositivity of Ti and in turn the formation of fewer defects in $BaTiO_3$ compared with the ferrite spinels.

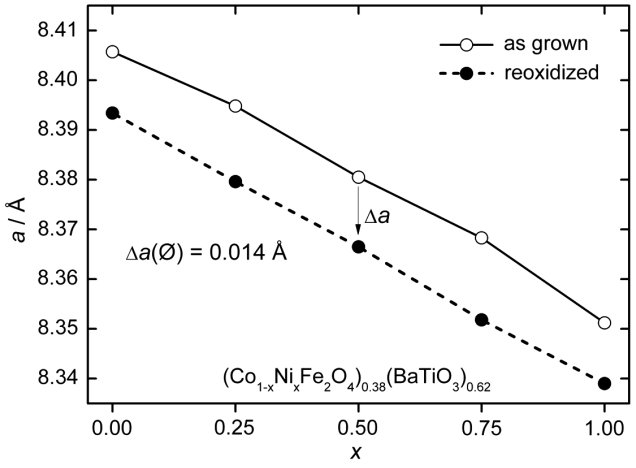

Figure 4. Unit cell parameters of $Co_{1-x}Ni_xFe_2O_4$ as function of Ni content.

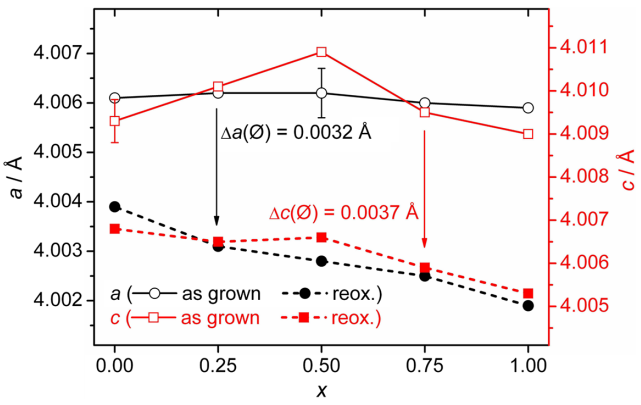

Figure 5. Unit cell parameters of $Ba_{0.97}Sr_{0.03}TiO_3$ with respect to the Ni content x in $Co_{1-x}Ni_xFe_2O_4$.

2.2. Thermal Analysis and Magnetic Properties

For a more detailed study of the oxygen defect healing, the as-grown samples were investigated by thermogravimetric (TG) analysis in oxygen. A magnet was attached under the furnace creating an extra attractive force on the ferrimagnetic spinel phase, which vanishes at the Curie temperature, resulting in an apparent weight loss. In turn, the thermogravimetric experiments can be used both for the investigation of the oxygen defects and the determination of the magnetic transition temperature T_C. As an example, the TG curve for the $Co_{0.75}Ni_{0.25}Fe_2O_4/Ba_{0.97}Sr_{0.03}TiO_3$ composite is shown in **Figure 6**.

In the heating regime, the weight loss at roughly 400 °C results from the ferrimagnetic → paramagnetic phase transition. The reoxidation of the composite mainly happens between 600 and 950 °C and is basically completed after the dwell time of 30 min at 950 °C. This rather fast defect healing can be explained by the high oxide ion mobility in spinel-type oxides. For example, for single-crystalline $(Ni_{0.68}Fe_{0.32})Fe_2O_4$, an oxygen diffusion coefficient of $D = 0.005 \times \exp\{-256\ \text{kJ mol}^{-1}\ \text{K}^{-1}/(RT)\}$ ($\text{cm}^2\ \text{s}^{-1}$) was found.[27] For polycrystalline $NiCr_2O_4$, a similar value of $D = 0.017 \times \exp\{-275\ \text{kJ mol}^{-1}\ \text{K}^{-1}/(RT)\}$ ($\text{cm}^2\ \text{s}^{-1}$) was reported.[28] These high mobilities allow an individual oxygen ion to travel a distance in the range of 1 µm within 1 h at 900 °C. The weight gain of 0.29 wt% corresponds to 0.04 oxygen per formula unit of $(Co_{0.75}Ni_{0.25}Fe_2O_4)_{0.38}(Ba_{0.97}Sr_{0.03}TiO_3)_{0.62}$. As both components may be oxygen deficient, it is difficult to derive a chemical composition for the as-grown material. Because during reoxidation, the relative change of the unit cell parameters of the ferrites (≈0.17%) is about twice the one of $Ba_{0.97}Sr_{0.03}TiO_3$ (≈0.09%), one might assign a defect ratio of 2/1 (given that the effect of an oxygen defect is equal in both phases). Assuming that the reoxidation product is free of oxygen defects, this leads to the compositions $Co_{0.75}Ni_{0.25}Fe_2O_{3.93}$ and $Ba_{0.97}Sr_{0.03}TiO_{2.98}$ for the two components in the as-grown sample. In contrast, if the uptake of oxygen is assigned completely to the spinel phase, the derived composition is $Co_{0.75}Ni_{0.25}Fe_2O_{3.90}$.

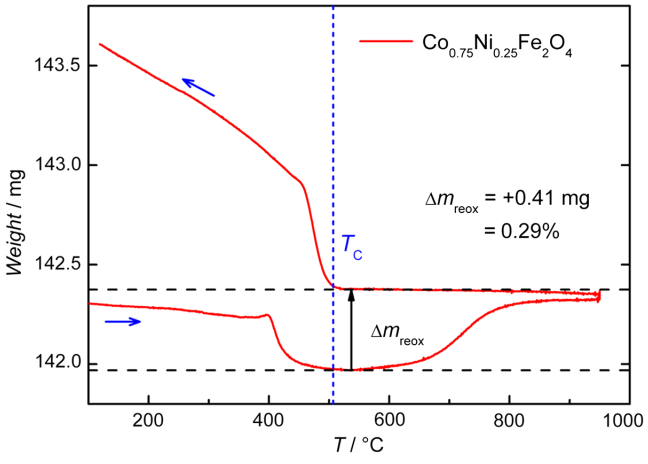

Figure 6. TG data of the as-grown $Co_{0.75}Ni_{0.25}Fe_2O_4/Ba_{0.97}Sr_{0.03}TiO_3$ composite during annealing in oxygen. The blue arrows indicate increasing and decreasing temperature.

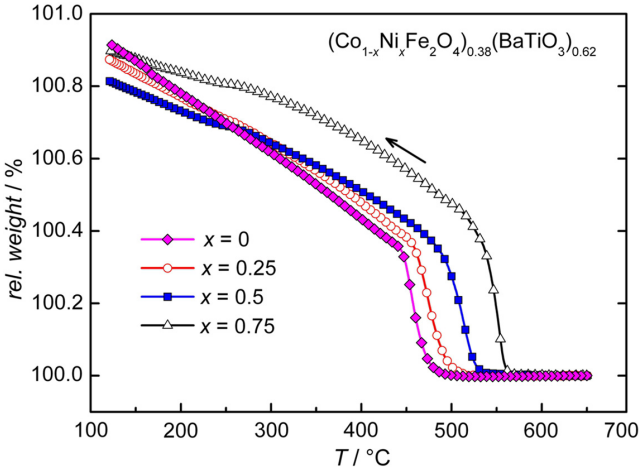

Figure 7. Thermogravimetric investigation in oxygen (cooling regime) of the different composite samples. Every 20th data point is shown as a symbol.

Upon cooling down from 950 °C, the weight remains constant until the Curie temperature $T_C = 510$ °C is reached, at which a pronounced increase in the measured weight is observed. The thermogravimetric investigation of the reoxidation has also been performed for the other samples. Because the weight gains assigned to the reoxidation are nearly the same ($x = 0.5$: $\Delta m = 0.29$ wt%, $x = 0.75$: $\Delta m = 0.28$ wt%,), only the cooling curves, which were used for the determination of T_C, are shown in **Figure 7**.

With increasing Ni contents, the weight gain associated with the ferrimagnetic ordering occurs at higher temperatures. The values of T_C determined from the onset of the weight increase are shown in **Figure 8** in comparison with the saturation magnetization (M_S) obtained from magnetization curves as shown in Figure S1, Supporting Information.

Both T_C and M_S show a nearly linear dependence on the Ni content. A similar behavior with only slightly different values has been observed for bulk samples of the $Co_{1-x}Ni_xFe_2O_4$ system (pure ferrite, no composite) underlining that the ferrite stoichiometries in our multiferroic composites obtained from the floating zone process are very close to the nominal ones.[29]

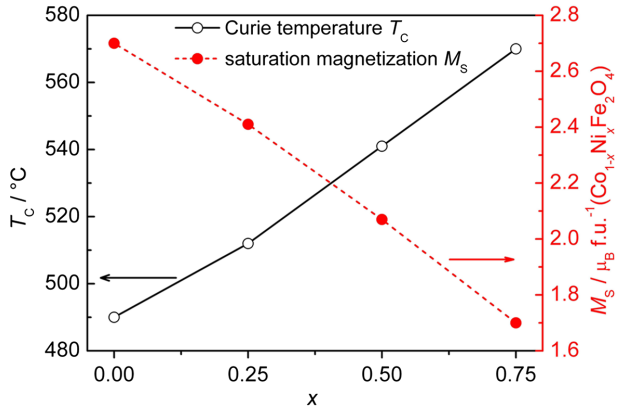

Figure 8. Curie temperatures and saturation magnetizations of the reoxidized samples.

2.3. ME Properties

Prior to the ME investigations, one reoxidized slice of each sample was poled, as described in Section 4. For a detailed investigation of the influence of the Ni substitution on the ME properties, ME values were measured as a function of the DC field, the frequency of the driving AC field and temperature.

In the following, the results for samples containing mixed ferrites ($x = 0.25$, 0.50, 0.75) are discussed in comparison with the ME properties of the $CoFe_2O_4/Ba_{0.97}Sr_{0.03}TiO_3$ composite ($x = 0$).[20] The sample containing pure nickel ferrite $NiFe_2O_4$ ($x = 1$) was found to be electrically conductive even after reoxidation and therefore could not be poled and measured.

The DC field-dependent measurements at 300 K were started at $H_{DC} = 10$ kOe. The magnetic field was decreased to $H_{DC} = -10$ kOe and reincreased to $H_{DC} = 10$ kOe. The amplitude and frequency of the AC field were fixed to 10 Oe and $f(H_{AC}) = 500$ Hz, respectively. The results are shown in **Figure 9**a.

All samples show the strongest ME response in the range $H_{DC} = \pm(2300–2500$ Oe). Also, their ME curves have very similar shapes; only the absolute values of α_{ME} change with the ferrite composition. This similarity is easier to be seen in the normalized data shown in Figure S2, Supporting Information. The maximum values are $\alpha_{ME}(max) = 1.3$, 1.1, 0.4, and 0.1 mV Oe^{-1} cm^{-1} for the samples with an Ni content of $x = 0$, 0.25, 0.50, and 0.75, respectively. This decrease in α_{ME} most likely stems from the declining magnetostriction in the mixed spinels $Co_{1-x}Ni_xFe_2O_4$ with higher x values.[30] The values for the remanent ME coefficient and the coercivity follow this trend, as shown in Figure 9b. The remanent values of α_{ME} are 3–4 times smaller than $\alpha_{ME}(max)$. The coercive fields decrease from 0.32 to 0.12 kOe for $x = 0$–0.75.

Our maximum α_{ME} values are comparable to the ones from the pioneering work of Van den Boomgaard et al. who reported ME coefficients of 1–4 mV cm^{-1} Oe^{-1}.[13,14] The only sample that showed a much larger value of 50 mV cm^{-1} Oe^{-1} had a strongly deviating composition and was later reported to consist of $BaTiO_3$, $CoFe_{2-x}Ti_xCo_xO_4$, and $BaFe_{12-2y}Co_yTi_yO_{19}$.[31]

In the current measurements, we found that the ME coefficients reach their highest and lowest values at the same magnetic field of $H_{DC}(max,min) = \pm(2300–2500$ Oe) independent of the sweep direction of H. This is in remarkable contrast to our earlier findings for eutectics containing pure $CoFe_2O_4$ for which a difference of about 600 Oe was observed between increasing and decreasing fields. Apparently, already the rather low substitution level of $x = 0.25$ in $Co_{1-x}Ni_xFe_2O_4$ suppresses this sweep-direction dependence occurring in $(CoFe_2O_4)_{0.38}/(Ba_{0.97}Sr_{0.03}TiO_3)_{0.62}$.[20]

In our experimental setup, a small AC field of 10 Oe is superimposed to the static magnetic field and drives the ME voltage. Therefore, the ME coefficient is expected to depend on the slope of the magnetostriction of the spinel and its maximum should occur at the maximum of $d\lambda/dH$. The magnetostriction of the $Co_{1-x}Ni_xFe_2O_4$ ($x = 0$, 0.2, 0.4, 0.6, 0.8, 1.0) system has been investigated in detail by Mathe and Sheikh.[30] Their results show that both the absolute value of λ and its slope decrease with higher Ni contents. While the change of slope is rather small between $x = 0$ and 0.2, the effect is more pronounced for higher nickel contents. Our measurements resemble this behavior, i.e., similar values of $\alpha_{ME}(max)$ were measured for $x = 0$ and $x = 0.25$ and higher Ni contents led to significantly smaller ME responses for $x = 0.50$ and $x = 0.75$. In addition, the magnetostriction curves given by Mathe et al. have their largest slopes between 1800 and 3000 Oe, which is roughly the same region in which $\alpha_{ME}(max)$ occurs in our investigations.[30]

Whereas Mathe et al. only report on the magnetostriction of the pure ferrites and also only for positive magnetic fields, a complete λ versus H hysteresis loop for a ceramic 0–3 composite of $(CoFe_2O_4)_{0.4}/(BaTiO_3)_{0.6}$ is given by Hrib and Caltun.[32] The ratio of spinel/perovskite is very close to ours and thus their results may be compared with the ME behavior of the sample with $x = 0$. As pointed out earlier, our ME signal is expected to be proportional to $d\lambda/dH$. For the comparison, we therefore fitted the data of Hrib et al. by two Lorentzian functions for the different field sweep directions. The normalized derivatives of these functions are shown in **Figure 10** in comparison with α_{ME} of our sample containing unsubstituted $CoFe_2O_4$ ($x = 0$). First, it is to be noted that a negative slope of $d\lambda/dH$ corresponds to positive values of α_{ME} (please note the inverted direction of the y-axis for $d\lambda/dH$). Second, the characteristic points of the two

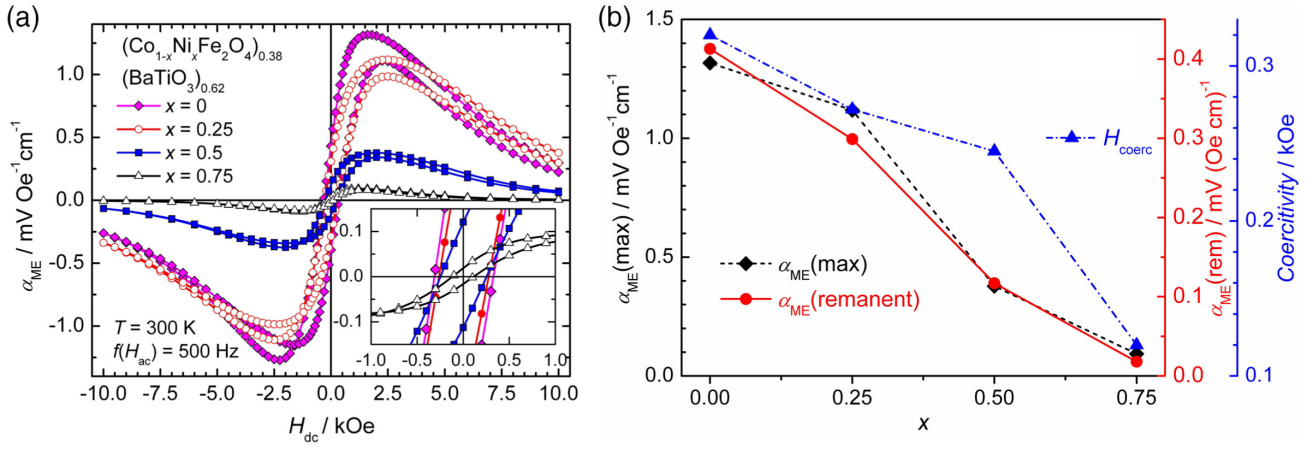

Figure 9. DC-field dependence of a) α_{ME} and b) extracted characteristic values of the series $(Co_{1-x}Ni_xFe_2O_4)_{0.38}/(Ba_{0.97}Sr_{0.03}TiO_3)_{0.62}$ with $x = 0$, 0.25, 0.50, and 0.75.

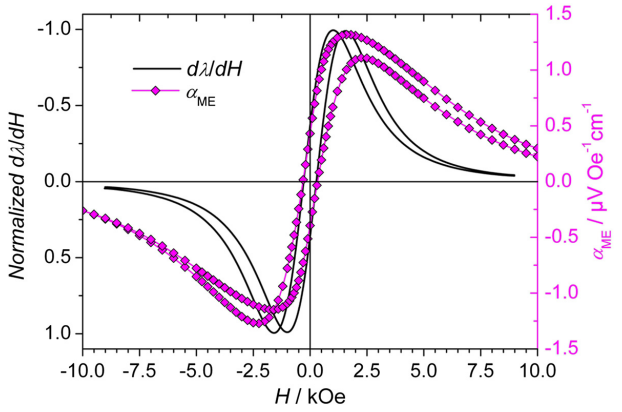

Figure 10. Comparison of the ME signal of $(CoFe_2O_4)_{0.38}/(Ba_{0.97}Sr_{0.03}TiO_3)_{0.62}$ with the derivative of λ measured for a ceramic $(CoFe_2O_4)_{0.4}/(BaTiO_3)_{0.6}$ composite.[32]

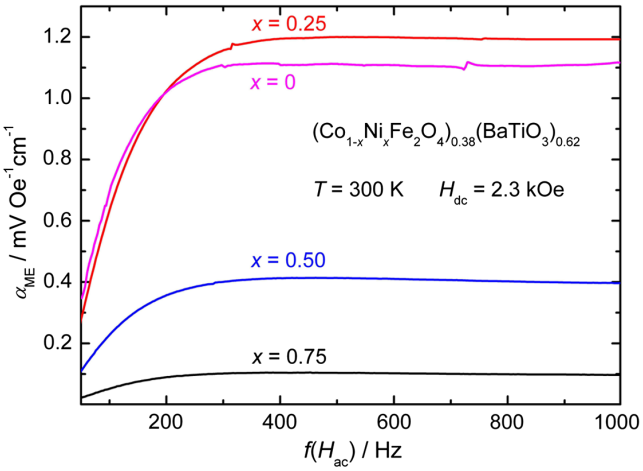

Figure 11. AC-frequency dependence of the ME coefficent.

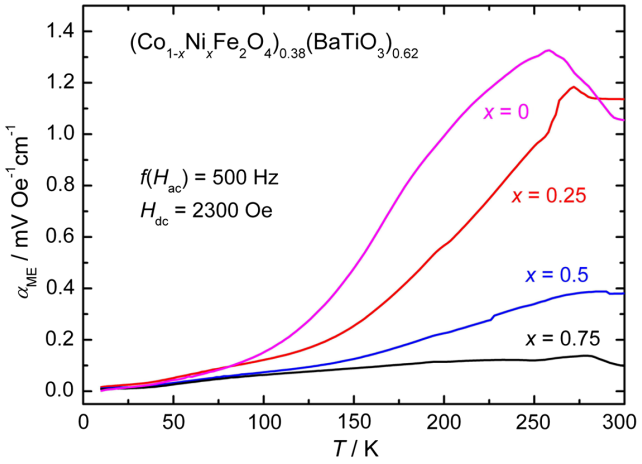

Figure 12. Temperature dependence of the ME coefficient.

curves correspond very well. That is, extreme values and zero crossings occur at similar magnetic fields and the remanent values are comparable too. Only at high fields deviations occur, where the decrease in the ME coefficient of the composite is far less pronounced. This difference can be explained by the clamping effect of the perovskite phase which is expected to be stronger in our crystallized samples compared with the ceramic one described in the literature.[32] One reason for a more effective clamping is the very low porosity of the melt-grown samples, which possess densities in the range of 94–98% of the crystallographic ones.[19] In addition, the epitaxial orientation of the two components corresponds to fewer defects (e.g., point defects or dislocations) at their interfaces leading to a better mechanical connection and in turn a stronger confinement. In this context, it is also worth mentioning that Hrib et al. observed strong deviations in the magnetostriction of their CFO/BTO composite in comparison with a pure $CoFe_2O_4$ sample that was processed identically. While for the 0–3 heterostructure, a Lorentzian-shaped field dependence was found, the magnetostriction curve for pure $CoFe_2O_4$ was bell-shaped (but not Gaussian-type as it is too broad at low fields) with zero slope at $H = 0$ and a hysteresis occurred at much higher magnetic fields. Thus, the α_{ME} field dependence of the 3–3 heterostructures obtained from eutectic crystallization can be explained by the magnetostriction of the spinel component, which is hindered by the clamping effect of the surrounding perovskite phase.

The dependencies of the ME effect on the frequency of H_{AC} and on temperature are shown in **Figure 11** and **12**. In these investigations, the static field was fixed to $H_{DC} = 2300$ Oe, i.e., close to α_{ME}(max) of the samples containing nickel ($x > 0$). Please note that for the sample containing unsubstituted $CoFe_2O_4$, the field of α_{ME}(max) is a little different (≈1600 Oe). Therefore, for this sample not the highest possible ME voltages have been measured. This is the reason for the apparently lower values of α_{ME} for $x = 0$ compared with $x = 0.25$ in Figure 11 and 12.

The values of α_{ME} increase with frequency and saturate between 300 and 400 Hz at $\alpha_{ME} = 1.2$, 0.4, and 0.1 mV Oe^{-1} cm^{-1} for $x = 0.25$, 0.50, and 0.75, corresponding to their maximum values (Figure 9). The smaller ME voltages in the low-frequency range (below ≈300 Hz) might be due to a partial internal discharge caused by the finite conductivity of the spinel phase. Because this discharge is rather slow, it becomes negligible at higher frequencies. On the other hand, it has been argued that in bulk composites charge accumulation at the interfaces of the two components can lead to an "inverse" Maxwell–Wagner-type relaxation, resulting in a charging of the capacitance (i.e., $BaTiO_3$) through the conductive ferrite. This effect first increases and finally saturates with rising frequency.[33] In our measurements, no resonance was detected in the investigated frequency range (50 Hz–1 kHz). Such resonances have been reported to occur between 15 and 430 kHz, a range unfortunately inaccessible with our setup.[34,35]

With rising temperature, the ME coefficient increases for all samples until its maximum is reached at 270–280 K (Figure 12). Up to room temperature, only a slight decrease is observed. The largest values for α_{ME} are found in the region of the orthorhombic/tetragonal phase transition of $BaTiO_3$ (265–280 K). This transition temperature is known to depend on various parameters such as crystallite sizes and substitutions. For example, Sr substitution or trace incorporations of Fe in $BaTiO_3$ both lower the phase transition temperature.[36] The temperature dependence of

α_{ME} basically reflects the piezoelectric behavior of $BaTiO_3$. Both piezo- and dielectric properties of $BaTiO_3$ result from the same ionic displacements (shift of titanium in the TiO_6 octahedra). Therefore, they are closely related and in turn α_{ME} can be compared with ε_r considering the slight strontium substitution ($Ba_{0.97}Sr_{0.03}TiO_3$), which is known to shift and broaden the phase transition temperatures.[37] The tetragonal, orthorhombic, and rhombohedral modifications of $BaTiO_3$ possess deviating permittivities due to the different displacements of Ti (along <001>, <110>, and <111> respectively; directions given with respect to the cubic perovskite structure). As shown in Figure 12, the orthorhombic/tetragonal phase transition can be detected by the ME voltage, whereas the rhombohedral/orthorhombic one is too small and broad to be seen. In contrast, for 0–3 composites of Ni/$BaTiO_3$ (without Sr substitution), both low-temperature structural transitions lead to clear signals in the ME voltage.[38] On the other hand, we cannot rule out the possibility that the temperature dependence of the magnetostriction may also play an important role. Temperature-dependent measurements of both the polarization and the magnetostriction are therefore planned for the future to distinguish the effects of the different parameters.

3. Conclusions

3–3 composites consisting of 62 mol% $Ba_{0.97}Sr_{0.03}TiO_3$ and 38 mol% $Co_{1-x}Ni_xFe_2O_4$ with $x = 0$, 0.25, 0.50, 0.75, and 1.0 were successfully grown by eutectic crystallization using the floating zone technique. The crystal lattices of the two components possess an epitaxial orientation, i.e., spinel(001)[100]|| perovskite(001)[100], on the micrometer scale. With the exception of the sample containing pure $NiFe_2O_4$, no impurity phases were detected. The linear dependencies of Curie temperatures, saturation magnetizations and ferrite cell parameters on the Ni content prove the successful substitution. Thermogravimetry in flowing oxygen shows a mass gain associated with the healing of oxygen defects leading to a pronounced increase of the electric resistivity. The absolute values of the ME coefficient decrease with rising Ni content. The DC field at which the maximum values of α_{ME} occur is independent of x and of the sweep direction of H, which is in a remarkable contrast to the unsubstituted $CoFe_2O_4/Ba_{1-x}Sr_xTiO_3$ eutectic. The field dependence of the ME coefficient resembles the derivative of the magnetostriction ($d\lambda/dH$) of particulate CFO/BTO ceramics, supporting the widely accepted interpretation of α_{ME} being the product property of the piezoelectric and piezomagnetic effect. Nearly constant ME coefficients were observed in a frequency range 400–1000 Hz without any resonances. The temperature-dependent ME investigations reveal local maxima at the orthorhombic/tetragonal phase transition of $Ba_{0.97}Sr_{0.03}TiO_3$.

After the first reports in the 1970s, the eutectic crystallization has barely been applied for preparing multiferroic composites and it has so far only been used for the system $CoFe_2O_4/BaTiO_3$. Here, we applied this approach for the first time to the substitution series $Co_{1-x}Ni_xFe_2O_4$. In further experiments, we plan to extend this promising synthesis technique toward other ferroelectric and ferromagnetic materials such as (Sr,Ba)Nb_2O_6 and $BaFe_{12}O_{19}$.

4. Experimental Section

Sample Preparation: Stoichiometric amounts of Co_3O_4 (≥99.7%, Alfa Aesar), NiO (>99.5%, Alfa Aesar), and Fe_2O_3 (≥99%, Sigma-Aldrich) were used for the synthesis of $Co_{1-x}Ni_xFe_2O_4$. $Ba_{0.97}Sr_{0.03}TiO_3$ with 1 mol% Ti-excess was prepared from $BaCO_3$ (≥99%, Solvay), TiO_2 (≥99%, Sachtleben), and $SrCO_3$ (≥99%, Merck). A detailed description of synthesis parameters such as heating rates, reaction temperatures, atmosphere, and the fabricating of sintered composite rods has been reported before.[19] The rods used for the floating zone melting consisted of 38 mol% ferrite and 62 mol% perovskite according to the eutectic composition of the $CoFe_2O_4/BaTiO_3$ system.[13]

A four-mirror floating zone furnace (CSC FZ-T-10000-H-HR-I-VPO-PC) equipped with 1500 halogen lamps was used to melt and recrystallize the $Co_{1-x}Ni_xFe_2O_4/Ba_{0.97}Sr_{0.03}TiO_3$ composites. Five different ferrite contents ($x = 0$, 0.25, 0.50, 0.75, 1) were prepared. A growth rate of 5 mm h^{-1} was used with seed and feed counter-rotating at 20 rpm. The floating zone process was conducted in nitrogen (5 N purity, gas flow 12 L h^{-1}). Slices of 0.7 mm thickness were cut out of the obtained crystal boules perpendicular to the growth direction. In contrast to our earlier experiments, higher temperatures (1173 K instead of 973 K) and pure oxygen (5 N purity, gas flow 9 L h^{-1}) instead of air were chosen during the 10 h reoxidation process.[19] These modifications were required because of the presence of Ni in the ferrite, which led to electrically conductive samples when reoxidation was conducted at lower temperatures or in air. Unless not otherwise stated, the reoxidized slices were used for all subsequent measurements.

Characterization: For SEM in combination with EDX, a Phenom ProX microscope was used (backscattered electron detector, acceleration voltage 15 kV). XRD measurements were conducted on a Bruker D8 Advance Bragg–Brentano diffractometer operating with Cu Kα radiation. Powder diffraction patterns were collected using a 1D silicon strip detector (LynxEye) in the 2θ range 10°–90° with a step size of 0.01° and a counting rate of 1 s per data point. The Thompson–Cox–Hastings pseudo-Voigt profile function was applied for Rietveld refinements with the FullProf Suite v.2.05. For single-crystal XRD an imaging plate diffractometer STOE IPDS-2T was applied (Mo Kα, graphite monochromator, 3 min $frame^{-1}$, $\omega = 0$–180°, $\Delta\omega = 1°$, $\varphi = 0°$ and 90°, $2\theta_{max} = 60°$). From the 360 measured frames, the reciprocal lattice was reconstructed with the STOE X-area software. Magnetic and ME measurements were performed in a Quantum Design Physical Property Measurement System PPMS-9 using a self-made setup described before for the ME investigations.[9] Magnetic hysteresis loops were recorded at room temperature with the magnetic field varying between −50 kOe and 50 kOe. For thermal analysis, a TA Instruments model 2950 was used. Samples were heated to 1223 K in oxygen (gas flow 4.5 L h^{-1}, heating rate of 10 K min^{-1}, dwell time 30 min). A baseline correction (measurement of an empty sample holder) was performed to account for the buoyancy effect. To determine the magnetic transition temperatures of the ferrites, a ring magnet was placed underneath the furnace.

Prior to the ME measurements, both sides of the reoxidized sample slices were contacted with sputtered gold electrodes of 100 nm thickness using a Cressington 108 auto sputter coater. Ferroelectric poling was conducted at room temperature for 12 h applying an electric field of 5 kV cm^{-1} with a current limited to 0.1 mA. For the ME measurements, a small AC field of 10 Oe was superimposed to the static magnetic field by a solenoid and the generated ME voltage was recorded applying a lock-in technique. Details of the DC-field-, AC-frequency-, and temperature-dependent ME measurements and the calculation of the ME coefficient (α_{ME}) are given in the literature.[20]

Supporting Information

Supporting Information is available from the Wiley Online Library or from the author.

Acknowledgements

This study was funded by the Deutsche Forschungsgemeinschaft (DFG, German Research Foundation)—project number 31047526—SFB 762, project A8.

Conflict of Interest

The authors declare no conflict of interest.

Keywords

composites, eutectic crystallization, interfaces, magnetoelectric properties, thermogravimetry

Received: September 30, 2019
Revised: February 27, 2020
Published online: April 24, 2020

[1] D. N. Astrov, *Sov. Phys. JETP* **1961**, *13*, 729.
[2] W. Eerenstein, N. D. Mathur, J. F. Scott, *Nature* **2006**, *442*, 759.
[3] M. Etier, V. V. Shvartsman, S. Salamon, Y. Gao, H. Wende, D. C. Lupascu, *J. Am. Ceram. Soc.* **2016**, *99*, 3623.
[4] M. Fiebig, *J. Phys. Appl. Phys.* **2005**, *38*, R123.
[5] V. V. Shvartsman, F. Alawneh, P. Borisov, D. Kozodaev, D. C. Lupascu, *Smart Mater. Struct.* **2011**, *20*, 075006.
[6] C.-W. Nan, M. I. Bichurin, S. Dong, D. Viehland, G. Srinivasan, *J. Appl. Phys.* **2008**, *103*, 031101.
[7] A. R. Iordan, M. Airimioaiei, M. N. Palamaru, C. Galassi, A. V. Sandu, C. E. Ciomaga, F. Prihor, L. Mitoseriu, A. Ianculescu, *J. Eur. Ceram. Soc.* **2009**, *29*, 2807.
[8] Y. Liu, Y. Wu, D. Li, Y. Zhang, J. Zhang, J. Yang, *J. Mater. Sci. Mater. Electron.* **2012**, *24*, 1900.
[9] T. Walther, U. Straube, R. Köferstein, S. G. Ebbinghaus, *J. Mater. Chem. C* **2016**, *4*, 4792.
[10] M. Bichurin, V. Petrov, A. Zakharov, D. Kovalenko, S. C. Yang, D. Maurya, V. Bedekar, S. Priya, *Materials* **2011**, *4*, 651.
[11] M. Etier, V. V. Shvartsman, Y. Gao, J. Landers, H. Wende, D. C. Lupascu, *Ferroelectrics* **2013**, *448*, 77.
[12] P. R. Mickel, H. Jeen, P. Kumar, A. Biswas, A. F. Hebard, *Phys. Rev. B* **2016**, *93*, 134205.
[13] J. Van den Boomgaard, D. R. Terrell, R. A. J. Born, H. Giller, *J. Mater. Sci.* **1974**, *9*, 1705.
[14] A. Van Run, D. R. Terrell, J. H. Scholing, *J. Mater. Sci.* **1974**, *9*, 1710.
[15] J. Echigoya, *J. Mater. Sci.* **2000**, *35*, 5587.
[16] J. Fukushima, K. Ara, Y. Hayashi, H. Takizawa, *Mater. Lett.* **2018**, *216*, 42.
[17] J. Fukushima, K. Ara, T. Nojima, S. Iguchi, Y. Hayashi, H. Takizawa, *Appl. Phys. Lett.* **2018**, *112*, 212903.
[18] N. Quandt, R. Roth, F. Syrowatka, M. Steimecke, S. G. Ebbinghaus, *J. Solid State Chem.* **2016**, *233*, 82.
[19] M. Breitenbach, S. G. Ebbinghaus, *J. Cryst. Growth* **2018**, *483*, 81.
[20] M. Breitenbach, H. Deniz, S. G. Ebbinghaus, *J. Phys. Chem. Solids* **2019**, *135*, 109076.
[21] R. M. Bozorth, J. G. Walker, *Phys. Rev.* **1952**, *88*, 1209.
[22] C. Deng, Y. Zhang, J. Ma, Y. Lin, C.-W. Nan, *Acta Mater.* **2008**, *56*, 405.
[23] J. Llorca, V. Orera, *Prog. Mater. Sci.* **2006**, *51*, 711.
[24] R. T. Shannon, *Acta Crystallogr. A* **1976**, *32*, 751.
[25] S. Singhal, J. Singh, S. K. Barthwal, K. Chandra, *J. Solid State Chem.* **2005**, *178*, 3183.
[26] H. T. Langhammer, T. Müller, T. Walther, R. Böttcher, D. Hesse, E. Pippel, S. G. Ebbinghaus, *J. Mater. Sci.* **2016**, *51*, 10429.
[27] H. M. O'Bryan, F. V. Dimarcello, *J. Am. Ceram. Soc.* **1970**, *53*, 413.
[28] W. D. Kingery, D. C. Hill, R. P. Nelson, *J. Am. Ceram. Soc.* **1960**, *43*, 473.
[29] Z. Dong, *J. Korean Phys. Soc.* **2008**, *52*, 4.
[30] V. L. Mathe, A. D. Sheikh, *Physica B, Condens. Matter* **2010**, *405*, 3594.
[31] J. Van den Boomgaard, R. A. J. Born, *J. Mater. Sci.* **1978**, *13*, 1538.
[32] L. M. Hrib, O. F. Caltun, *J. Alloys Compd.* **2011**, *509*, 6644.
[33] M. Bichurin, V. Petrov, in *Modeling of Magnetoelectric Effects in Composites*, Springer, Dordrecht, The Netherlands **2014**, pp. 45–56.
[34] W. P. Wang, H. Yang, T. Xian, R. C. Yu, *Chem. Phys. Lett.* **2015**, *618*, 72.
[35] S. Q. Ren, L. Q. Weng, S.-H. Song, F. Li, J. G. Wan, M. Zeng, *J. Mater. Sci.* **2005**, *40*, 4375.
[36] H. Ihrig, *J. Phys. C, Solid State Phys.* **1978**, *11*, 819.
[37] J.-H. Jeon, *J. Eur. Ceram. Soc.* **2004**, *24*, 1045.
[38] T. Buttlar, T. Walther, K. Dörr, S. G. Ebbinghaus, *Phys. Status Solidi B* **2020**, *257*, 1900622.